Indexing Diffraction Patterns

18

CHAPTER PREVIEW

Since the strength of TEM is that you can obtain both crystallographic data and an image from the same part of your specimen, a method for interpreting the DP is essential. The first step in any interpretation is to index your pattern. You can proceed in several ways, depending on how much information you already know about your specimen. We will begin the chapter by considering the experimental approach with the aim of being able to identify shortcuts whenever possible. The experienced microscopist will readily identify many patterns just by looking at them, but will still need to index new patterns or to identify unfamiliar ones. The fastest and most efficient experimental approach may take advantage of several concepts covered in the preceding two chapters and the following three.

Using the DP, we can identify the crystal (which we often already know) and its orientation. The positions of the allowed $hk\ell$ reflections are characteristic of the crystal system. Indexing associates each spot in the DP with a plane, $(hk\ell)$, in the crystal. From the indexing of the spots, you can deduce the orientation of the crystal in terms of the zone axis $[UVW]$ in which the indexed planes lie. This direction is normal to the plane of the DP and antiparallel to the electron beam. It is convention to define $[UVW]$ as the beam direction. If you want to know the orientation relationship between two crystals, you need to know more than one $[UVW]$ for each crystal.

D. B. Williams et al., *Transmission Electron Microscopy*

© Springer Science+Business Media New York 1996

Indexing Diffraction Patterns

18

18.1. CHOOSING YOUR TECHNIQUE

The technique you choose to study your specimen will depend on what you *want* to learn and what you *can* learn. For example, if you want to learn about the structure of a particular region, you may find moiré fringes (Chapter 27) or HRTEM (Chapter 28) more appropriate. We can summarize the possibilities as a function of the grain size of the material. Basically there are two approaches:

- You can focus the beam on a small area of your specimen to form a convergent-beam electron-diffraction (CBED) pattern (see Chapters 20 and 21).
- You can spread the beam to give nearly parallel illumination and then use an aperture to select an area in the first image formed by the objective lens (the SAD patterns of Chapters 9 and 11).

Let's consider the specimen characteristics:

- The grain size may be very small, ≤10 nm. This is a problem! However, in this case you probably won't want to know the orientation of a particular grain but will instead be interested in knowing the texture of the material. It is also probable that the electron beam will pass through several such grains in a typical thin specimen, in which case you can't analyze an individual grain.
- The grain size is between 10 nm and ~100 nm. Here CBED may be useful because it gives you a small probe. However, much of the benefit of CBED comes from having specimen thicknesses which are > 100 nm; this thickness depends on the structure factor (atomic number) of your specimen. With modern TEMs C_s and λ are so small that you might be able to use SAD in this range if you're careful, as we saw in Table 11.1.
- The grain size is in the range 100 nm to ~2 μm. In this situation, SAD can be used quite routinely in a modern TEM. You must be aware of the limitations and be prepared to unravel a complex DP. Because of errors due to C_s and Δf, the problem will be distinguishing which spots arise from the area you selected and which spots arise from neighboring areas.
- The specimen is uniformly thin with grain size >2 μm. This type of specimen is just a simpler version of the last case. You should have no problem in applying SAD techniques even at lower voltages and in older microscopes. Now CBED will be very useful in examining local changes *within* a grain.
- The grains of interest are large (>2 μm, even better if they are >5 μm) with both thin areas (<100 nm to 300 nm thick, depending on the material) and areas which are sufficiently thick for Kikuchi lines to be visible (see next chapter). Now you can use any of these techniques, except texture analysis, which becomes more difficult! For the latter, you should now consider the electron-backscatter pattern (EBSP) technique in an SEM (Randle 1993).

In this chapter we'll concentrate on the hands-on approach to SAD analysis and leave CBED to Chapters 20 and 21. We can't give you a foolproof guide since your technique will depend on your specimen.

18.2. EXPERIMENTAL TECHNIQUES

By now you should know how the experimental camera length (L) compares to the value you read from the micro-

scope. You also know how the pattern is rotated with respect to the image as the magnification changes, unless your particular TEM automatically compensates for this rotation. You've checked that you haven't missed a 180° inversion; leading researchers have missed this in the past. Go back to Sections 9.3 and 11.10 if you need more details on the practical steps involved in obtaining SAD patterns.

You can vary L but your pattern may rotate as you do so. We generally use a value of ~500 mm for SAD, but that will depend on your microscope, whether you want to see detail in the HOLZ and on the interplanar spacings in your specimen. It's good practice to choose a particular value of L and always use that value for your SAD patterns with a particular instrument/specimen combination. You may want to increase L for special high-resolution diffraction, but you'll give up a large number of other reflections and enlarging the photographic film will almost always provide the magnification you need.

Tilting and rotating the specimen. One of the biggest assets of the TEM is that you can monitor the DP as you tilt or rotate your specimen. Rotating the pattern requires a rotation holder, which is ideal if you want to align a particular reflection parallel to the tilt axis, especially for a side-entry holder. This alignment is particularly helpful in stereomicroscopy (see Chapter 31). Tilting the specimen is far more common than rotating, since all side-entry holders automatically have one tilt axis parallel to the specimen rod. We discussed the importance of eucentricity in Chapter 9.

> Tilting the specimen changes the diffraction conditions and may change the focus.

It is good practice to note the tilt settings whenever you are recording images. If you want to use these settings to give a rough estimate of how far you're tilting the specimen, you should remember that there may be some backlash due to mechanical hysteresis. So you will always need to approach a particular setting from the same tilt direction if you need to be exact. In the next chapter, we'll describe how we use Kikuchi maps to guide us as we tilt the specimen. If you don't have Kikuchi lines because your specimen is too thin, or too bent, you can still use the idea. Set up a particular excited beam and tilt the specimen so that one particular beam remains excited. What you are doing is tilting the specimen so that the same plane remains nearly parallel to the electron beam.

Tilting the beam. If you are really interested in examining the detail present in the DP and the image is less important, you can change the diffraction conditions in a very controlled and reversible way by tilting the beam using the DF deflection coils. You can be very precise and there is no problem with backlash. To increase your accu-

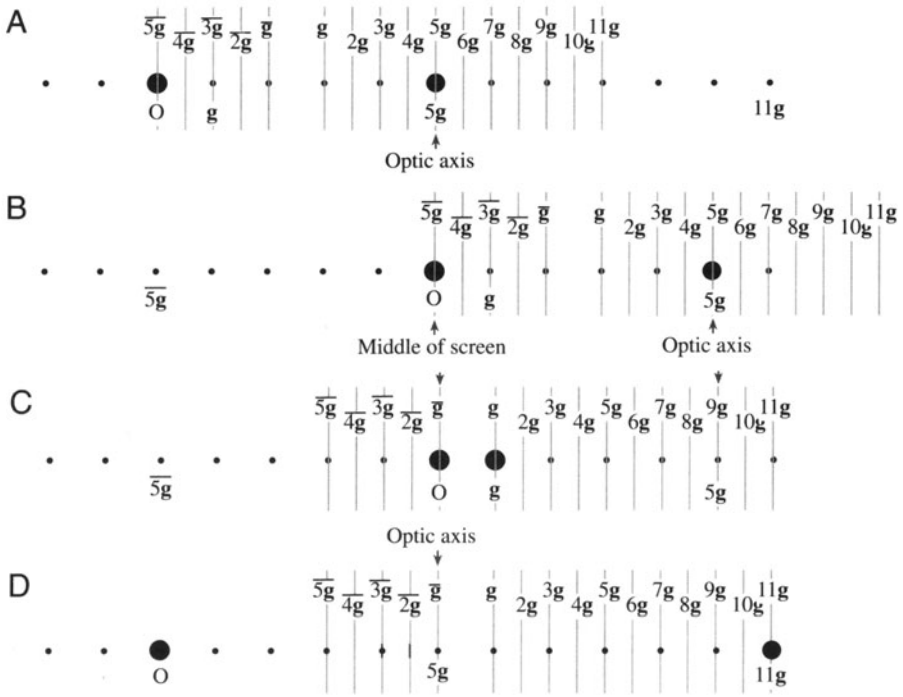

Figure 18.1. The steps used to excite a high-order reflection. (A) Tilt the beam so **5g** is on axis and strongly excited. (B) Translate the pattern so O is in the middle of the screen. (C) Tilt the specimen to excite **g** (the Kikuchi lines move). (D) Tilt the beam so that **5g** is back on axis and **11g** is strong.

racy, you may want to increase L. This technique is particularly helpful when you want to examine the effect of small changes in **s** on the appearance of diffraction spots. For example, if you want to excite the eleventh-order reflection 11**g** but you can't see 11**g**, use the following approach, shown in Figure 18.1:

- Tilt the beam using the dark-field deflection coils so that 5**g** is on axis (Figure 18.1A).
- Use the translation coils on the projector lens to bring the direct beam back to the middle (so that you can see it easily) (Figure 18.1B).
- Tilt the specimen so that **g** is excited (Figure 18.1C).
- Then tilt the beam with the DF coils and translate the pattern with the projector lens so that 5**g** is back on the optic axis; 11**g** should now be excited (Figure 18.1D).

We'll develop other variations of this technique in Chapter 19, and we'll see in Chapter 26 that the situation in Figure 18.1 does arise in weak-beam microscopy at higher voltages.

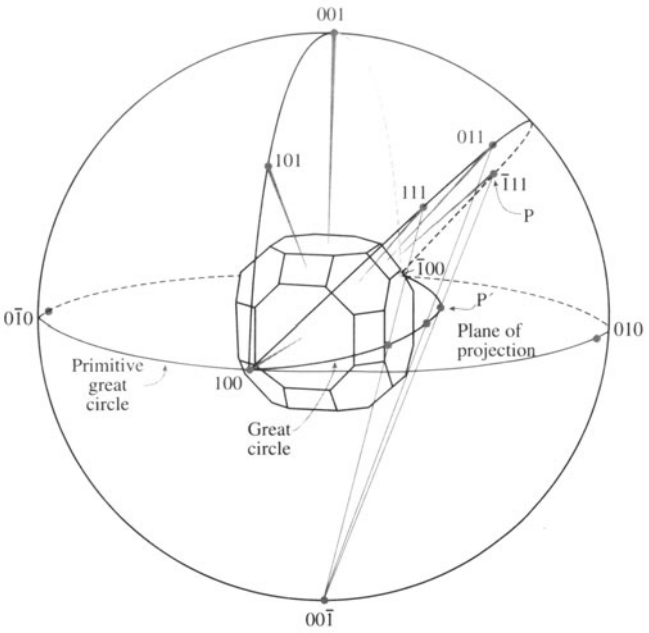

Figure 18.2. The stereographic projection. The crystal is at the center of the sphere. Normals to the crystal planes are projected until they intercept the sphere at P, then projected back to the south pole $(00\bar{1})$ of the sphere. Where this projected line crosses the equatorial plane at P' is the point that uniquely represents the original plane on the crystal. Note that planes in the same zone on the crystal project as a line of longitude on the sphere, called a great circle, and project as the arc of a circle on the equatorial plane, whose circumference is called the primitive great circle.

18.3. THE STEREOGRAPHIC PROJECTION

Diffraction patterns not only tell us the direction of the electron beam, but also the complete orientation of that region of the specimen illuminated by the beam. If we have a grain boundary present in the specimen we can determine the orientation of both grains and the plane of the interface. What we often want to know is how the two grains are related to one another. We need a method for visualizing this relationship; this is where the stereographic projection is an invaluable aid (Johari and Thomas 1969). Like other tools, you'll have to understand it and use it before you fully appreciate its value. We strongly recommend that you take time out to do this if you're not already familiar with the construction. Any introductory crystallography text is a good place to start and several are listed in the general references.

The construction. Imagine a crystal located inside a sphere as shown in Figure 18.2. Draw a line normal to each crystal plane from the center of the sphere (the sphere of projection) to intersect the sphere at point P in the northern hemisphere; the cross-section view may be easier to visualize. Now draw a line from the south pole to point P.

This line cuts the disk containing the equator at the point P'. The disk is the stereographic projection and the point P' *uniquely* represents the plane whose radial normal cuts through P. If P is in the southern hemisphere, draw the line from the north pole instead and identify this P' on the projection with a circle instead of a dot.

Look again at the crystal; it's cubic to keep it simple but the construction is completely general. The normals to the planes (100), (111), (011), and $(\bar{1}11)$ and all lie on the circumference of a circle around the sphere of projection. In this special case, all of the points on this circumference project onto a great circle on the stereographic projection whose circumference we call the "primitive" great circle. The Wulff net shown in Figure 18.3 shows 90 such great circles all passing from the north pole to the south pole and another around the equator: a great circle always passes through opposite ends of a diameter in the projection. These are the familiar lines of longitude on the globe. Circles on the sphere which do not contain the center of the sphere are smaller; they also project as circles called the small circles, which if concentric with the primitive are familiar as lines of latitude. (Note, however, that most small circles are not concentric with the primitive.) We can then rotate the Wulff net as we wish, to realign our great circles.

- We can represent plane normals (also called poles) and directions on the same projection even if they are not parallel to one another. Bet-

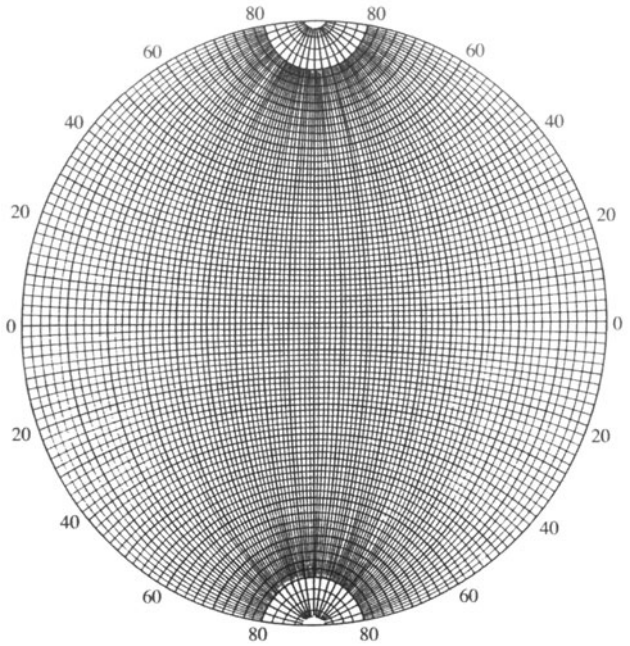

Figure 18.3. A Wulff net which contains 90 great circles like the one in Figure 18.2; each great circle is 2° apart so the net covers 180°. The only great circle that actually appears as a circle in the net is the circumference of the projection, called the primitive great circle. Points on this circle represent planes whose normals are 90° from the north pole of the sphere (which projects in the center of the Wulff net). Therefore, all distances on the net are proportional to angles in real space but only correspond exactly to angles around the primitive great circle.

ter still, we can read off the angles between them. Remember, in general, that the normal to the plane $(hk\ell)$ is parallel to the direction $[hk\ell]$ only for cubic materials.

- The zone axis is always 90° away from any plane normal in its zone. All the plane normals in a particular zone, $[UVW]$, will lie on a single great circle; these are the possible diffracting planes for that zone (i.e., the $[UVW]$ beam direction). So if $[UVW]$ is in the center of the projection, the $hk\ell$ reflections will be around the circumference of the projection (the primitive great circle).
- The angle between any two planes is the angle between their plane normals, measured along a great circle using the Wulff net.
- We can use the same construction to summarize all the symmetry elements of any particular crystal system.

Several examples of stereographic projections are shown in Figure 18.4. Look at the Wulff net and check some simple facts. For example, for the cubic system, check which poles are 90° away from the $[\bar{0}01]$ direction. How large is the angle between $(0\bar{1}1)$ and (011)? How would this angle change if the material were forced to be tetragonal with $c/a > 1$? What happens in this case to the $(1\bar{1}1)$ pole or the $(1\bar{1}0)$ pole? Now consider the more extensive plot shown in Figure 18.5. If the specimen is cubic with the [001] foil normal, what pole would you tilt to if you wanted to form an image with the $0\bar{2}2$ reflection? (One answer is the [011] zone axis, but why?) For the same specimen, if you want to excite the $\bar{1}11$ reflection, tilt toward the $[\bar{1}10]$ zone axis with the 220 reflection excited, not toward the $[1\bar{1}0]$ zone axis.

- You could work this out using equations, but the stereographic projection tells you what to do while you are sitting at the microscope.
- If you are working with a noncubic material, buy a large Wulff net and construct your own stereographic projection; you can buy standard projections for cubic materials. Use a program like Desktop Microscopist or EMS to help you

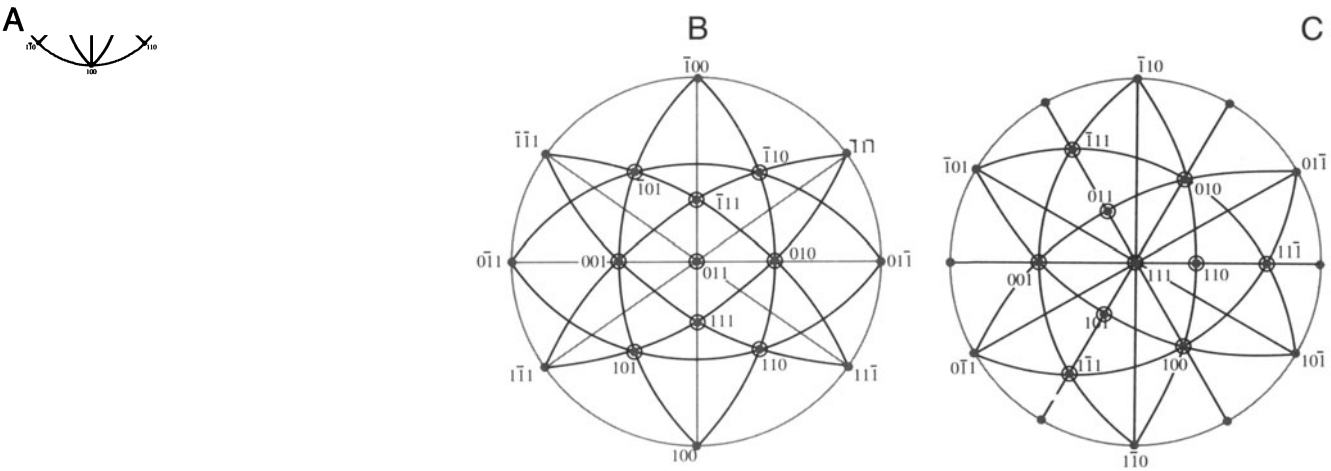

Figure 18.4. Some standard cubic stereographic projections. The pole in the center defines each projection, so these are 001, 011, and 111.

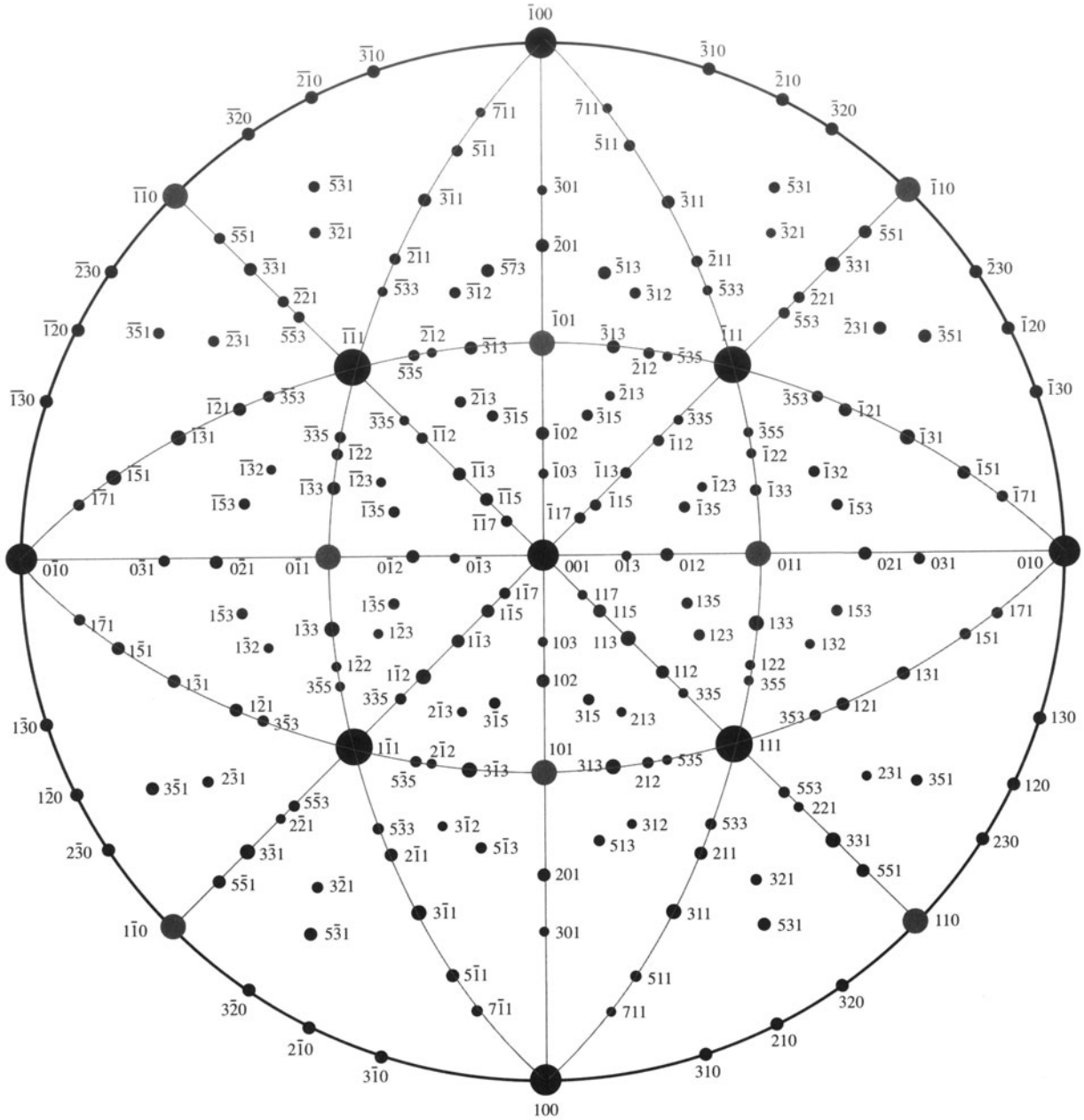

Figure 18.5. The stereographic projection for a cubic foil with a [001] normal, assuming the beam is down [001] also. If you want to form an image with the $0\bar{2}2$ reflection, you need to tilt the specimen so the $0\bar{1}1$ pole rotates until it is on the primitive, i.e., it is 90° from the beam direction. To do this you need to tilt about an axis that is 90° from the $0\bar{2}2$ reflection, such as the [100], [111], [311], zone axes.

plot the points, or download appropriate freeware from the WWW.

18.4. INDEXING SINGLE-CRYSTAL DIFFRACTION PATTERNS

Remember the fundamental relationship in a DP (refer back to Chapter 9)

$$Rd = \lambda L \qquad [18.1]$$

Any distance, R, which we measure on the DP is related to a specific spacing in the crystal, d. Since λL is a constant, we can measure several values of R and know that

$$R_1 d_1 = R_2 d_2 = R_3 d_3 = R_4 d_4 = \cdots \qquad [18.2]$$

Therefore the ratio of any two R values gives the ratio of the d-spacings. If you know the lattice parameter of your

Table 18.1. The Selection Rules for Cubic Crystal Structures

bcc		fcc		Diamond cubic	
$h^2+k^2+\ell^2$	$hk\ell$	$h^2+k^2+\ell^2$	$hk\ell$	$h^2+k^2+\ell^2$	$hk\ell$
2	110				
		3	111	3	111
4	200	4	200	4	200
6	211				
8	220	8	220	8	220
10	310				
		11	311	11	311
12	222	12	222		
14	321				
16	400	16	400	16	400
18	411				
	330				
		19	331	19	331
20	420	20	420		
22	332				
24	422	24	422	24	422
26	431				
		27	511	27	511
		27	333	27	333
30	521				
32	440	32	440	32	440

crystal, then you know the allowed reflections and only certain d-spacings will be associated with diffraction spots. Table 18.1 illustrates allowed and forbidden reflections for some cubic systems. Rules for more crystal systems are given back in Table 16.2.

Once you have tentatively identified possible values for $\mathbf{g}_1$ and $\mathbf{g}_2$, you need to cross-check your answers using the angles between the $\mathbf{g}$ vectors (i.e., the angles between the plane normals). The fully indexed patterns at the end of this chapter show the principal interplanar angles and the principal ratios of $\mathbf{g}_1/\mathbf{g}_2$. Hence, in practice, you will rarely have to measure more than two or three spacings in order to index a particular zone-axis DP. However, if your specimen is not oriented close to a zone axis, you'll need to look ahead to Section 18.8.

> Remember to check the consistency of your indexing using the Weiss zone law. Each $hk\ell$ reflection must lie in the $[UVW]$ zone, i.e., $hU + kV + \ell W = 0$.

The angle between normals to the planes $(h_1k_1\ell_1)$ and $(h_2k_2\ell_2)$ is ϕ; the angle between directions $[U_1V_1W_1]$ and $[U_2V_2W_2]$ is ρ. You can work these out and cross-check them with your DPs. These are standard equations in many texts, e.g., Edington (1976) and Andrews *et al.* (1971). You'll probably find that the most useful are the equations for the cubic system

$$\cos\phi = \frac{h_1h_2 + k_1k_2 + \ell_1\ell_2}{\left(h_1^2+k_1^2+\ell_1^2\right)^{\frac{1}{2}}\left(h_2^2+k_2^2+\ell_2^2\right)^{\frac{1}{2}}} \quad [18.3]$$

$$\cos\rho = \frac{U_1U_2 + V_1V_2 + W_1W_2}{\left(U_1^2+V_1^2+W_1^2\right)^{\frac{1}{2}}\left(U_2^2+V_2^2+W_2^2\right)^{\frac{1}{2}}} \quad [18.4]$$

Remember that you can always work out these expressions for any crystal system using the equation for the dot product of the two appropriate vectors.

In principle, if we don't know the crystal structure, we can still work out the d-spacings of the diffracting planes using equation 18.1. However, you should remember that SAD is not the most accurate method for determining the spacing of lattice planes, $d_{hk\ell}$, or the angles between them, ϕ. SAD is generally very good at distinguishing patterns, but it completely fails when the difference between the two patterns is a 180° rotation as occurs in some patterns of polar material, like GaAs.

To summarize, tilt your specimen to a low-index pole, set $\mathbf{s} = 0$ for the innermost reflections, and record the SAD pattern. Repeat the exercise using higher-order reflections after tilting the specimen to set $\mathbf{s} = 0$. These measurements will be more accurate, but only if you make sure that $\mathbf{s} = 0$. The discussion on relrods in Chapter 16 told you that both d and ϕ could be seriously in error if reflections are not set to have $\mathbf{s} = 0$, especially since you've probably tilted the specimen.

So far, you have only indexed one DP. You'll probably need more than one to determine orientation relation-

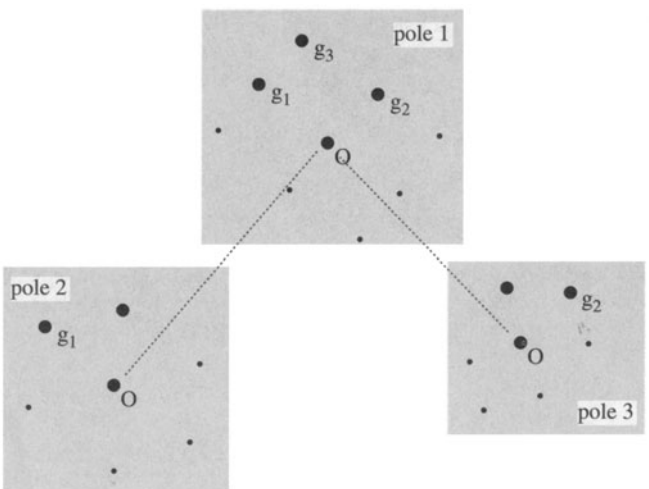

Figure 18.6. How to confirm your indexing of reflections and poles by tilting to other poles: Start with $\mathbf{g}_1$ and $\mathbf{g}_2$ strongly excited at pole #1. Tilt to pole #2, keeping $\mathbf{g}_1$ strong, then go back to pole #1 and tilt to pole #3, keeping $\mathbf{g}_2$ strong. Index all the strong reflections each time, measure the tilt angles between each reflection, and estimate the tilt between poles.

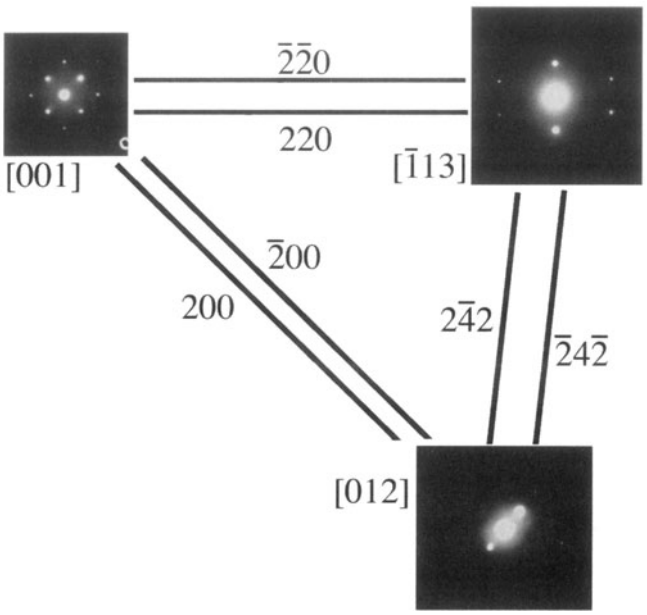

Figure 18.7. A practical illustration of the procedure described in Figure 18.6 for an fcc material, in this case MgO.

ships. While you're at the microscope, tilt to pole #2, keeping $\mathbf{g}_1$ (see Figure 18.6) strongly excited. Repeat the indexing procedure. Go back to pole #1 and tilt to pole #3, keeping $\mathbf{g}_2$ strongly excited. You can repeat this indexing as many times as you wish. The important idea is that you now have angular measurements allowing you to cross-check your determination of both $\mathbf{g}_1$ and $\mathbf{g}_2$ and the zone axes. Of course, the task is simple for an fcc crystal, as you can see in Figure 18.7, which is an experimental illustration of this procedure. The challenge comes when the crystal has less symmetry. If you already know the crystal structure, then you should plot out the most important poles, relating their orientations to one another (more on this in Section 18.9 and Chapter 19), and pay particular attention to the information from systematic absences as occur when the structure factor is zero.

The golden rule is: make the task as easy as possible while you're at the microscope. Record all the DPs you might need during your TEM session.

18.5. RING PATTERNS FROM POLYCRYSTALLINE MATERIALS

Diffraction from polycrystalline specimens can be viewed in much the same way as X-ray diffraction from powders. For a completely random polycrystal, we rotate the reciprocal lattice about all axes and produce a set of nested spheres. When we intersect these spheres with the Ewald sphere (which, in the TEM, approximates to a plane) we will see the rings that are recorded in powder patterns.

If the polycrystal is textured, then there is usually one special plane which is nearly common to all the grains. We then rotate the reciprocal lattice about the lattice vector normal to this plane and produce a set of circles in reciprocal space, as shown in Figure 18.8. If we are examining cubic materials, the reciprocal lattice vector $\mathbf{g}_{hk\ell}$ will be parallel to the direction $[hk\ell]$ in real space. Otherwise, this will not generally be the case.

Since the grains are small, all the reciprocal lattice points will be broadened by the shape effect; so will the sphere or circles for the polycrystals.

The DP in either of these examples appears as shown in Figures 18.9A and B, which differ because the grain size is different. A larger grain size gives a more speckled pattern.

You can distinguish the pattern produced by a textured specimen from one produced by a random polycrystal by tilting. If the specimen is textured, the rings become arcs as shown in Figure 18.10A together with the Ewald sphere construction in Figure 18.10B. You can locate the grains which give rise to the arcs by forming a DF image with the arc. In the example shown in Figure 18.10C, these

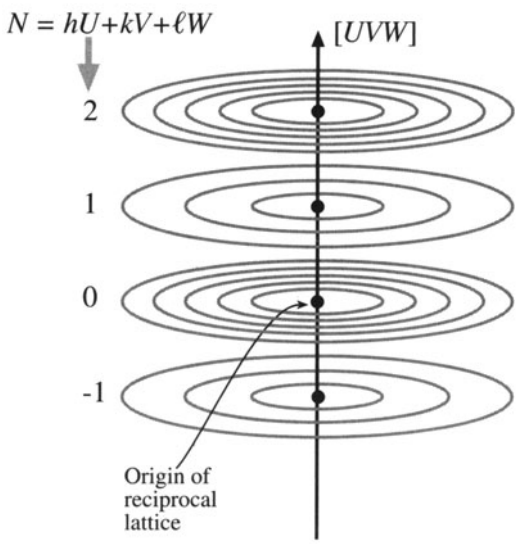

Figure 18.8. The generation of a set of circles in reciprocal space by a textured polycrystal. When the reciprocal lattice is rotated about a particular direction $[UVW]$ (in this case the normal to the texture plane), each Laue zone (N = 1, 2, etc.) produces a set of concentric circles for each allowed reflection in each zone.

A

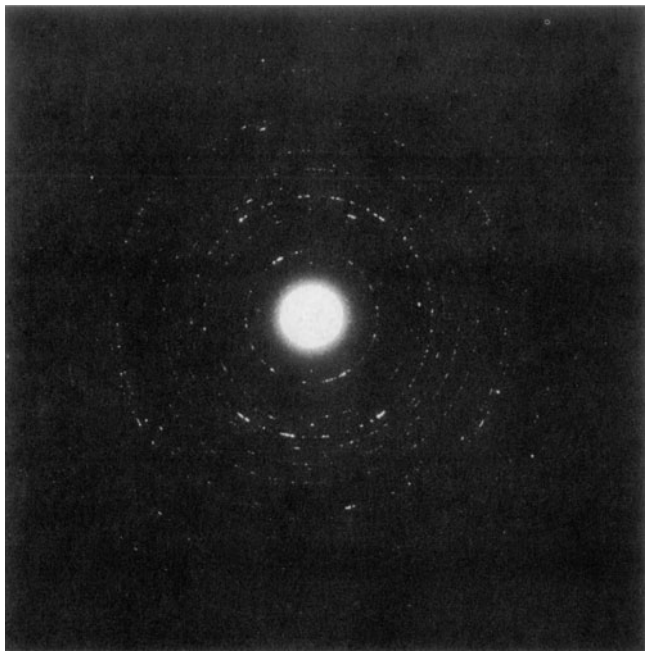

B

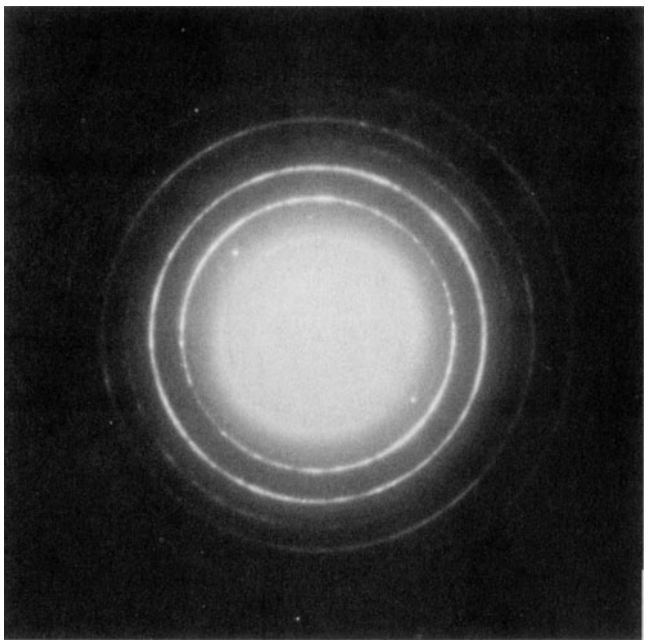

Figure 18.9. Ring diffraction patterns from polycrystalline foils. In (A) the grain size is larger than in (B), so the rings are made up of discrete spots. A finer grain size, as in (B), produces a more continuous ring pattern, but the widths of the rings of diffracted intensity in fact become broader and can be used as an inverse measure of the grain size.

oriented grains are uniformly distributed, but you might encounter a situation where this is not the case.

Figures 18.10D and E emphasize that these patterns can be quite varied. In this case, the specimen is α-Ag_2Se, which is textured about an axis that is *inclined* to the beam. When the Ewald sphere cuts the circles now, it produces elongated spots which lie on an ellipse. Vainshtein *et al.* (1992) point out that all the "spots" on one ellipse can be indexed with the same *hk* indices but a different ℓ, and call such a pattern an oblique-textured electron DP (OTEDP). You should also be careful in indexing these textured patterns since not all possible $d_{hk\ell}$ values need be present, depending on the texture plane.

There is more information in these patterns. Like a powder pattern you could estimate the grain size from the width of the rings, but it's more direct to just look at the DF image. You can see kinematically forbidden rings because you don't necessarily have single scattering from each grain.

One challenging application of these patterns concerns nanocrystalline materials, which fall into our smallest range of ~10-nm grain size. Careful DF imaging combined with HRTEM is probably optimal, but you need to look for clustering of similarly oriented grains.

18.6. RING PATTERNS FROM AMORPHOUS MATERIALS

The first question you have to answer on this topic is one of the most difficult, namely, is the material really amorphous or is it (sub)nanocrystalline? Actually, this question is still debated when discussing both amorphous materials and, more intensely, oxide and metallic glasses.

> The DP from an amorphous material looks similar to that from polycrystalline material, but the rings are broader and there is no speckle.

Rudee and Howie (1972) showed that electron scattering from regions of ≤15-Å diameter could be coherent. Graczyk and Chaudhari (1973) proposed modeling these materials as random networks. If we are careful, we can learn quite a lot about the structure of amorphous materials, but we should first say what we mean by "amorphous".

Figure 18.10. (A) A textured ring pattern where the rings are more intense over a certain angular range. (B) The corresponding interception of the Ewald sphere (plane) with the reciprocal lattice. (C) A DF image of the textured grains, taken from a brighter portion of one of the *hkℓ* rings, showing an equiaxed structure. In (D) the specimen is textured about a direction at an angle to the beam, so the Ewald sphere creates elongated spots or arcs in the diffraction pattern (E).

A

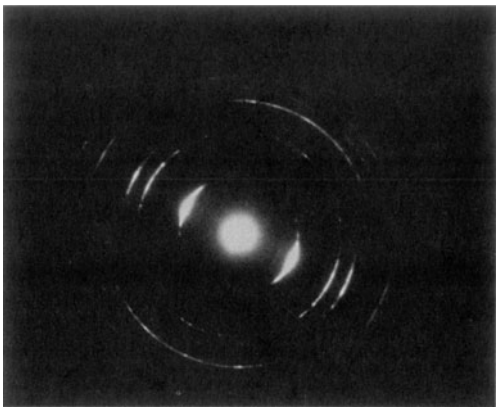

B

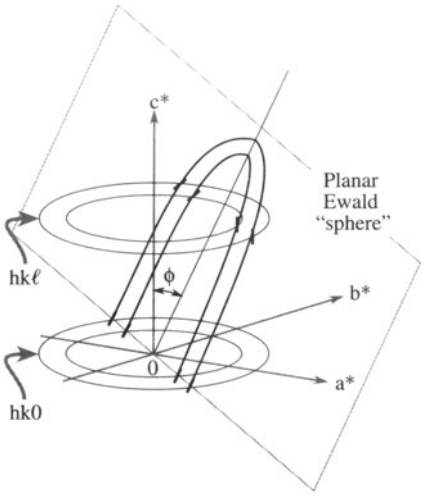
c*
Planar
Ewald
"sphere"
hkℓ
ϕ
b*
0
a*
hk0

C

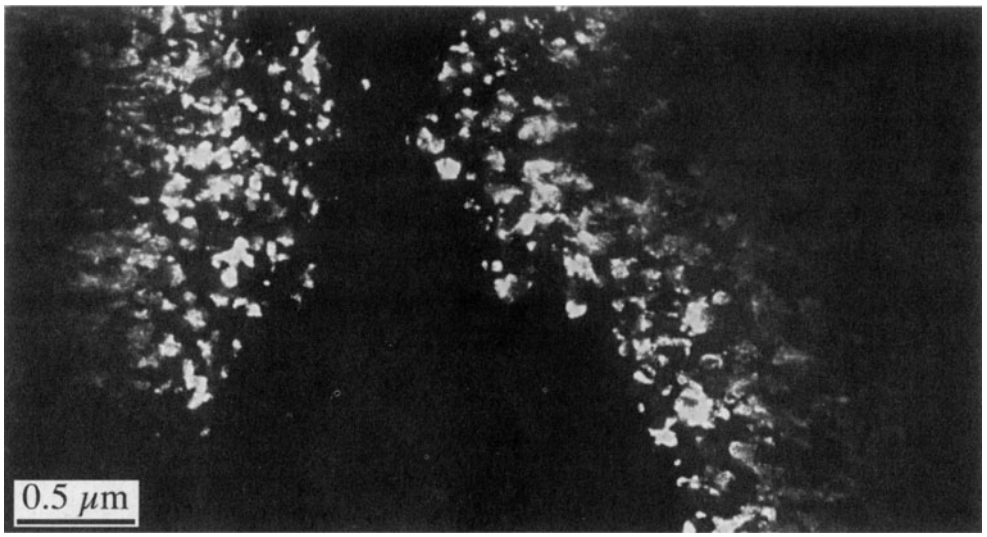
0.5 μm

D

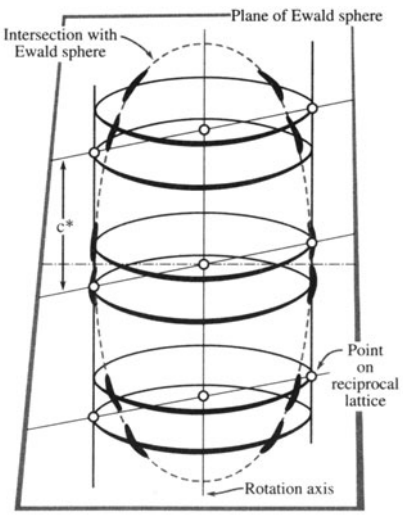
Plane of Ewald sphere
Intersection with
Ewald sphere
c*
Point
on
reciprocal
lattice
Rotation axis

E

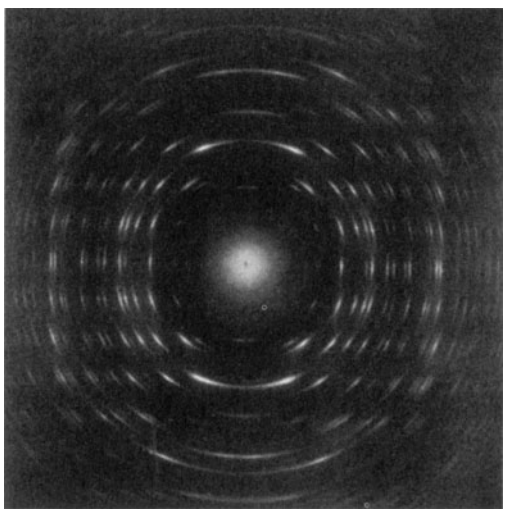

An amorphous material is one where the locations of the neighboring atoms are defined by a probability function such that the probabilities are never unity.

This idea is best illustrated by a plot of the probability which we call the *radial distribution function* (RDF). The RDF, $\rho(r)$, is the probability, per unit element of volume, that an atom will be found at a distance r from another atom. The first example in Figure 18.11A compares the curves for liquid sodium and crystalline sodium; the numbers on the crystalline curve remind us that in the crystal each sodium has eight nearest neighbors, etc. The second plot, Figure 18.11B, shows the RDF for vitreous silica. This time the peaks are associated with distances between different pairs of Si and O atoms. The features to notice are:

- The two curves both show definite peaks.
- The two curves are different.

Some diffraction theory. Since these materials are so different, we'll give a brief introduction to the theory of scattering from amorphous materials. We make the assumption that the electron beam is only scattered once; this is kinematical, but more realistic than for crystals at the Bragg condition. Following Howie (1988) we express the kinematical intensity, $I(\mathbf{k})$, by the expression

$$I(\mathbf{k}) = |f(\mathbf{k})|^2 \sum_{i,j} e^{i2\pi\mathbf{k}\cdot(\mathbf{r}_i - \mathbf{r}_j)} \qquad [18.5]$$

Here we assume that there are N identical atoms contributing to the scattered intensity and they are located at the different $\mathbf{r}_i$ positions.

The $f(\mathbf{k})$ terms are the atomic scattering amplitudes, with $\mathbf{k}$ reminding us that there is an angular dependence on f. If the material is isotropic, we can simplify equation 18.5 as follows

$$I(\mathbf{k}) = N|f(\mathbf{k})|^2\left(1 + \frac{F(\mathbf{k})}{k}\right) \qquad [18.6]$$

where

$$F(\mathbf{k}) = \sum_{i \neq j} e^{i2\pi\mathbf{k}\cdot(\mathbf{r}_i - \mathbf{r}_j)} \qquad [18.7]$$

$$F(\mathbf{k}) = k \int \rho(r) e^{i2\pi\mathbf{k}\cdot\mathbf{r}} dV \qquad [18.8]$$

$$F(\mathbf{k}) = 4\pi \int_0^\infty \rho(r) \sin(2\pi kr)\, r\, dr \qquad [18.9]$$

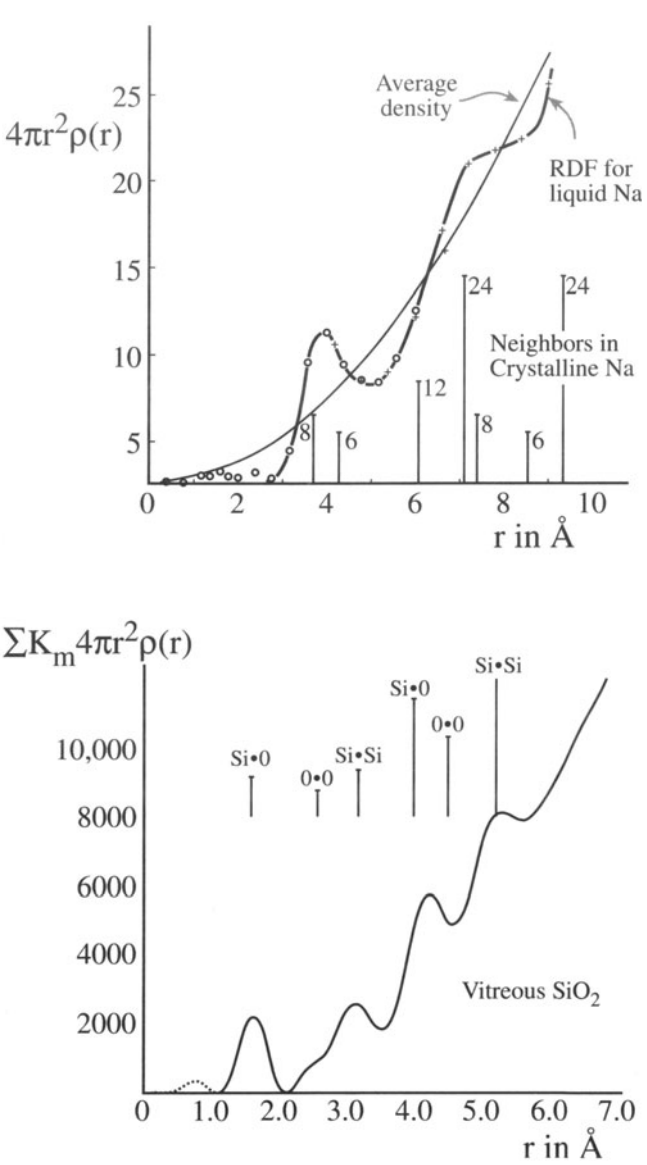

Figure 18.11. (A) Radial distribution function for liquid Na and the average density curve, superimposed on the distribution of the nearest neighbors in crystalline Na (vertical lines). (B) The RDF for vitreous SiO_2 is peaked at distances that represent various spacings between atoms.

The term $\rho(\mathbf{r})$ is the RDF. Equation 18.9 can be inverted to give an expression for ρ

$$\rho(r) - \rho_0 = \frac{1}{r}\int_0^\infty F(\mathbf{k}) \sin 2\pi kr\, dk \qquad [18.10]$$

The RDF can be obtained directly from DPs, and this process is enhanced if the patterns are energy-filtered to remove inelastic contributions (see Chapter 40 and the work of Cockayne *et al.* 1991). Software to determine the RDF

is listed back in Section 1.5. Then we can obtain DPs shown graphically in Figures 18.12 and 18.13. Alternatively, we can rearrange equation 18.6 again to give a "reduced intensity function" as illustrated by the work of Graczyk and Chaudhari (1973). Graczyk and Chaudhari showed clearly that the structure correlation can extend to 15 Å or more.

To summarize this discussion, the scattering theory is well known but the capability for routinely removing the inelastic contribution is only now becoming available and is still not commonplace. Probably the best way to answer whether a material is nanocrystalline or amorphous will come from a combination of SAD and EELS. A BF image of amorphous material is generally uninformative (Figure 18.14A), but if you try to form a DF image you will see a speckle of white spots against a dark background, as shown in Figure 18.14B. The size of the speckle increases as the defocus increases, so be wary of interpreting your image in terms of the size of regions in the amorphous structure. Hollow-cone DF imaging, where you use an annular C2 aperture as shown in Figure 18.14C, gives even more, and finer, "structure" in the image. The fact that you can produce this type of speckled contrast is important because you may well want to study small particles (e.g., catalysts) supported by an amorphous film. In such a case, you need to know what the image of the support film looks like before you add a new component.

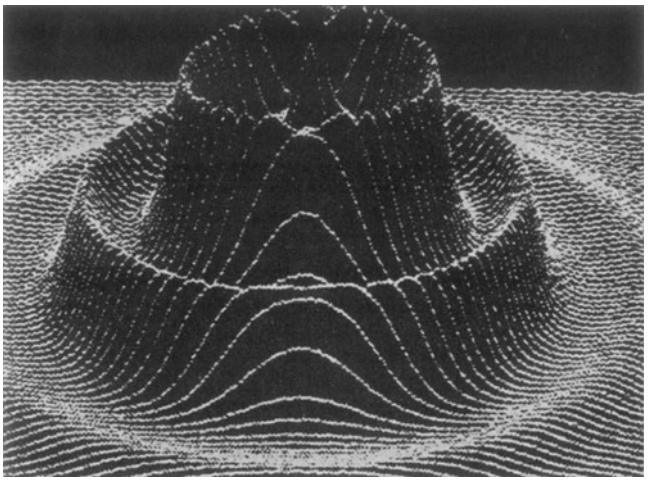

Figure 18.13. A computer plot of the diffracted-intensity distribution from an amorphous structure, showing diffuse rings of intensity. The direct-beam intensity is off scale.

Glass and grain boundaries. Another area where it is important to know whether or not an amorphous material is present occurs in the analysis of grain boundaries in ceramic materials. The technique, known as diffuse-dark-field imaging, essentially forms an image from the region in the SAD pattern where the amorphous ring would be, if glass were present. We'll return to this topic in Chapter 31.

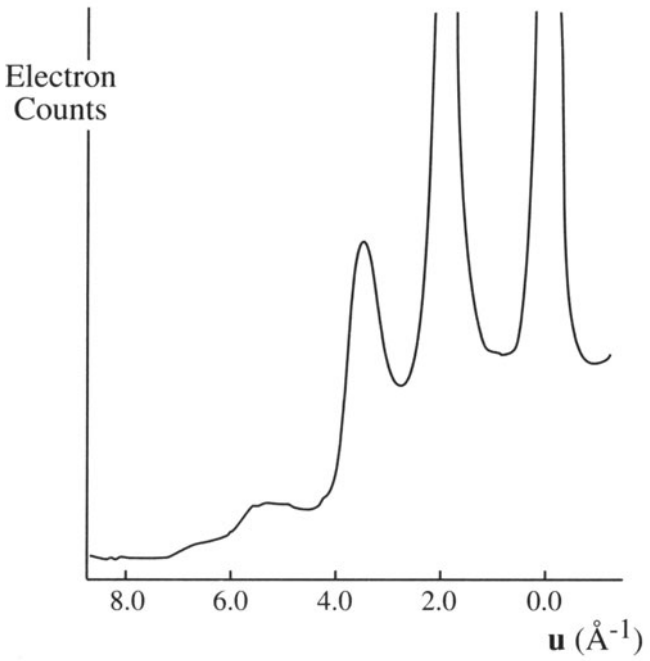

Figure 18.12. An intensity profile across an energy-filtered diffraction pattern from amorphous Si obtained by scanning the pattern across the entrance slit to a serial EELS spectrometer and recording only the elastic (on-axis) electrons.

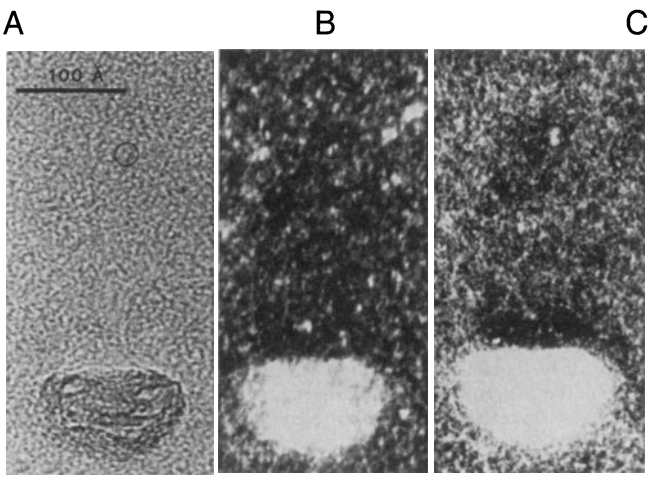

Figure 18.14. (A) BF image of amorphous carbon. (B) DF image from the diffuse diffracted intensity taken with a defocused beam. (C) A hollow-cone image showing more structure.

18.7. DOUBLE DIFFRACTION

Double diffraction occurs when a diffracted beam traveling through a crystal is rediffracted either within the same crystal or when it passes into a second crystal. If the initial diffraction vector of the beam is $\mathbf{g}_1$ and it is rediffracted by reflection $\bar{\mathbf{g}}_2$, then the resultant diffraction vector of the double-diffracted beam is $(\mathbf{g}_1\text{-}\mathbf{g}_2)$. If $\mathbf{g}_2$ is not an allowed reflection in the first crystal, the double-diffracted beam is characteristic of neither the first nor the second crystal.

Reflections attributable to double diffraction are a common feature of DPs recorded from two-phase materials exhibiting epitaxy or topotaxy including, e.g., oxidized metallic specimens. Quite complicated patterns may be formed, requiring careful analysis to distinguish the "real" reflections from the double-diffraction reflections. Double diffraction is directly responsible for the moiré effect in the electron images which we will discuss in Chapter 27. As an example of this effect, we'll consider small α-Fe_2O_3 (hematite) islands grown on a single-crystal α-Al_2O_3 (alumina or sapphire) substrate (Tietz *et al.* 1995), as shown in Figure 18.15A. The position of the double-diffraction spots relative to the hematite and alumina reflections actually changed depending on whether the islands were on the top or bottom surface of the specimen. This particular top–bottom effect can be derived from simple geometry; however, dynamical-diffraction effects must also be considered when the materials are thicker.

Figure 18.15B shows the [0001] SAD pattern recorded from one of these α-Fe_2O_3 particles. The closest reflections to the direct beam are the six $\{11\bar{2}0\}$ reflections. The next closest reflections are the six $\{3\bar{3}00\}$ reflections, only four of which are visible in the figure. Double-diffraction spots are visible around each of these primary reflections. They also surround the direct beam, although they are hidden by the flare from that beam in Figure 18.15B.

Figures 18.15C and D show enlargements of regions near the $\{11\bar{2}0\}$ reflections in the [0001] SAD patterns recorded when the hematite island was on the top surface in (C) and on the bottom surface of the sapphire in (D). Both $\mathbf{g}$ and $\bar{\mathbf{g}}$ reflections are shown for the two cases. In (C) the ring of six double-diffraction spots surrounds the Al_2O_3 reflection while in (D) the double-diffraction spots surround the Fe_2O_3 reflection.

The same observation can be made for the $\{\bar{3}300\}$ regions of the SAD patterns, as shown in Figures 18.15E and F. In this case, an inner ring of double-diffraction spots (small filled circles) with the same spacing and orientation as the double-diffraction reflections in Figures 18.15C and D are still visible, as are the outer rings of spots (large

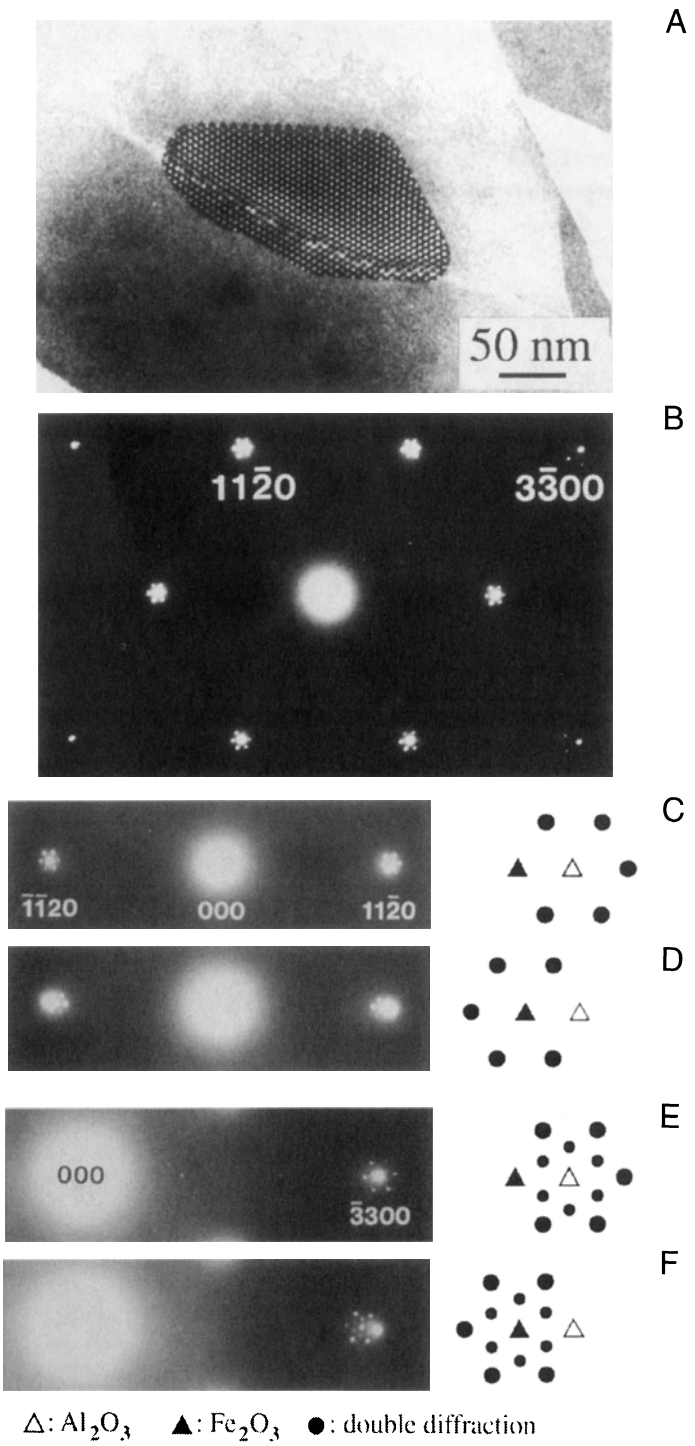

Figure 18.15. (A) BF on-axis image of a particle of α-Fe_2O_3 on α-Al_2O_3. (B) [0001] SAD pattern from α-Fe_2O_3 showing double-diffraction spots around the $\{11\bar{2}0\}$ and $\{3\bar{3}00\}$ reflections. (C) Enlargements of regions near the $(11\bar{2}0)$ reflections when the hematite island was on the top surface. (D) Enlargements of regions near the $(11\bar{2}0)$ reflections when the hematite island was on the bottom. (E) Enlargements of regions near the $(\bar{3}300)$ reflections when the hematite island was on the top surface. (F) Enlargements of regions near the $(\bar{3}300)$ reflections when the hematite island was on the bottom.

filled circles). In general, the outer ring of double-diffraction spots is more intense than the inner ring.

Both this top–bottom effect in particular, and double diffraction in general, can be explained by the simple geometric analysis we show in Figure 18.16; the bottom crystal is Al_2O_3, which has the smaller lattice parameter and therefore has the larger reciprocal lattice vectors. Double-diffraction spots can be formed around the primary hematite reflection, $\mathbf{g}_H$, by two different routes:

- $2\mathbf{g}_H + \bar{\mathbf{g}}_A$ (A: alumina, H: hematite) gives a double-diffraction spot just inside $\mathbf{g}_H$.
- $\bar{\mathbf{g}}_H + 2\mathbf{g}_A$ gives a double-diffraction spot just outside $\mathbf{g}_H$.

These two routes at first appear to be equivalent. However, if we take into account the curvature of the Ewald sphere, then the deviation parameters of the two routes are very different. In the case of diffraction through the upper crystal, the deviation parameter of the $2\mathbf{g}$ beam is slightly more than twice that of the $\bar{\mathbf{g}}$ beam. This difference will not significantly affect the intensities from a very thin epilayer due to streaking of the reciprocal lattice spots parallel to the beam direction (the shape-factor effect).

Now we can analyze the effects of diffraction through the lower crystal:

- Draw the reciprocal lattice with the origin of the Ewald sphere at $2\mathbf{g}_H$ for the first case and on $\bar{\mathbf{g}}_H$ in the second.
- Keep the radius of the Ewald sphere unchanged since only elastic interactions are considered.
- The incident beam for the lower crystal is in the $2\mathbf{g}$ or $\bar{\mathbf{g}}$ directions for the two cases.
- The height of the ZOLZ is slightly different in the two cases since the deviation parameter at the origin must be zero.

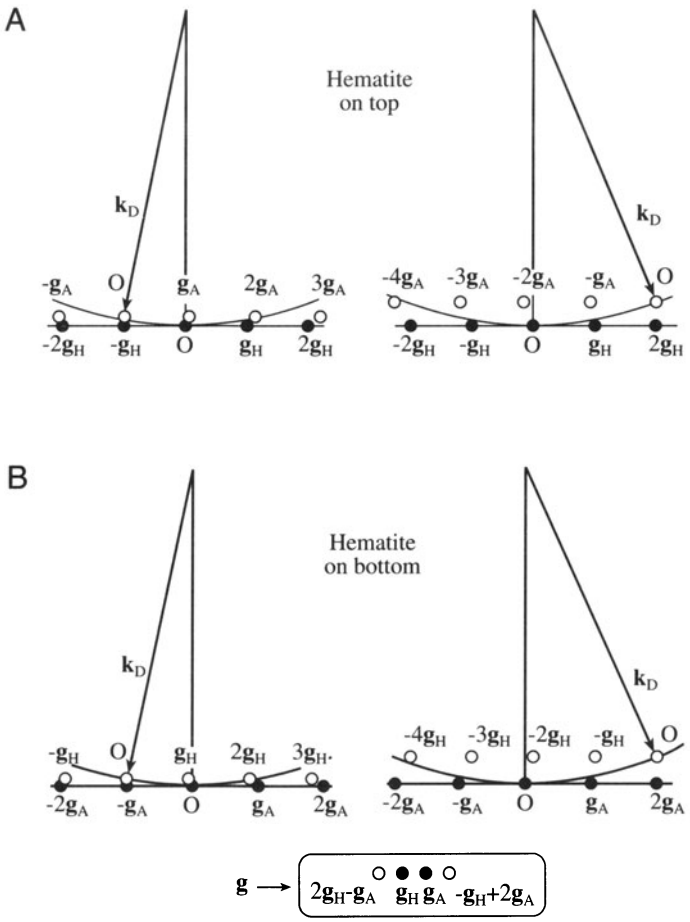

Figure 18.16. Top–bottom effect in double diffraction. The pattern depends on which of the two crystals is on top. In (A) α-Fe_2O_3 particles are on top of the Al_2O_3; in (B) Fe_2O_3 particles are below the Al_2O_3. Two nonequivalent paths for double diffraction are shown.

You can see from Figure 18.16A that the deviation parameter for $2\mathbf{g}_A$ is approximately zero, whereas for $\bar{\mathbf{g}}_A$ it is of the same order as $\mathbf{g}_H$. The total deviation parameter is thus much smaller for the second route than the first. A similar analysis for the inverted structure is shown in Figure 18.16B. In both cases the deviation parameter for the route $\bar{\mathbf{g}}$ (upper) plus $2\mathbf{g}$ (lower) produces a much smaller deviation parameter than the route $2\mathbf{g}$ (upper) plus $\bar{\mathbf{g}}$ (lower). So the double-diffraction spot, which occurs on the same side of the diffraction spot from the upper crystal as the diffraction spot from the lower crystal, will be more intensely excited than the double-diffraction spot which occurs on the opposite side.

> In two dimensions, for thin films, the strongest double-diffraction spots will always be those arranged symmetrically around the diffraction spot from the lower crystal.

For thicker layers, the relative intensity of the $\bar{\mathbf{g}}$ and $2\mathbf{g}$ beams will vary as dynamical-diffraction effects occur. We can simulate the DPs from these structures using the MacTempas program (see Chapter 29). The top–bottom effect is evident in the case of 2.7 nm of hematite on 13 nm of alumina, but only just discernible for the case of 2.6 nm of alumina on 13.5 nm of hematite. In the latter case, the dynamical-diffraction effects are stronger.

We'll return to this topic in Chapter 27 when we discuss moiré fringes. We have made this analysis a little more complicated than usual since we have considered the

details of where the spots will actually be found. You can make this process simpler:

- Trace the patterns from each crystal.
- Then construct a new pattern using each diffracted beam from the upper crystal as an incident beam for the lower crystal.

The extent of the moiré pattern gives you an idea of just how strong dynamical scattering is, even for thin films! More examples of double diffraction are given in Edington (1976).

18.8. ORIENTATION OF THE SPECIMEN

Once you have identified three **g** vectors $\mathbf{g}_1$, $\mathbf{g}_2$, and $\mathbf{g}_3$ in a single-crystal DP, you can calculate the direction of the beam **B**. You can actually estimate **B** to within about 10° from the vector cross product as follows

$$\mathbf{B} = \mathbf{g}_1 \times \mathbf{g}_2 = \begin{bmatrix} \mathbf{i}_1 & \mathbf{i}_2 & \mathbf{i}_3 \\ h_1 & k_1 & \ell_1 \\ h_2 & k_2 & \ell_2 \end{bmatrix} \qquad [18.11]$$

$$= (k_1\ell_2 - k_2\ell_1,\ \ell_1 h_2 - \ell_2 h_1,\ h_1 k_2 - h_2 k_1) \qquad [18.12]$$

For the three-beam case, you can determine **B** with an accuracy of ~ 3°. You first need to make sure that the three vectors are taken in the correct order. Draw a circle through these three reflections: if O is inside the circle, then the **g** vectors should be numbered counterclockwise; if O is outside, number them clockwise. Check your labeling; the determinant of the matrix in equation 18.13 should be positive

$$\mathbf{g}_1 \cdot (\mathbf{g}_2 \times \mathbf{g}_3) = \frac{1}{V}\begin{bmatrix} h_1 & k_1 & \ell_1 \\ h_2 & k_2 & \ell_2 \\ h_3 & k_3 & \ell_3 \end{bmatrix} \qquad [18.13]$$

Now we can write a weighted-average expression for **B**

$$\mathbf{B} = \frac{\mathbf{g}_2 \times \mathbf{g}_3}{|\mathbf{g}_1|^2} + \frac{\mathbf{g}_3 \times \mathbf{g}_1}{|\mathbf{g}_2|^2} + \frac{\mathbf{g}_1 \times \mathbf{g}_3}{|\mathbf{g}_3|^2} \qquad [18.14]$$

A convention: The vector **B** points up the column. It is normal to the emulsion side of a photographic negative. The electron beam travels along the direction -**B**.

In Figures 18.17–18.19, we illustrate some of the most useful DPs for bcc, fcc, and hcp crystals. You can extend these patterns as far as you wish using vector addition; remember the reflections correspond to reciprocal-lattice *vectors*. For example, in Figure 18.17C

$$(12\bar{1}) = (110) + (01\bar{1}) \qquad [18.15]$$

You can extend the patterns in this way and then apply the selection rules to find the corresponding patterns for Si, etc., using the specific examples as a guide.

- bcc real space → fcc reciprocal space.
- fcc real space → bcc reciprocal space.

Take the example used by Edington (1976), as shown in Figure 18.20 for an fcc crystal. Measure the distances to the reflections *x*, *y*, and *z*. Since the material is fcc, we can ratio d^2 values to find suitable indices or use a calibrated camera length. Thus we find that plane A = $(4\bar{2}0)$, B = (111), and C = $(\bar{3}31)$; check that the angles are correct using

$$\cos(\phi_{AB}) = \frac{\mathbf{g}_A \cdot \mathbf{g}_B}{|\mathbf{g}_A||\mathbf{g}_B|} \qquad [18.16]$$

and so on for ϕ_{BC} and ϕ_{CA}. You should immediately recognize that this is the $\pm[12\bar{3}]$ pole, but continue. Now you can plug these indices into equation 18.11 or 18.14 to show that **B** = $[\bar{1}\bar{2}3]$.

Finally, use the [001] stereographic projection. Draw a great circle that passes through the (111), $(2\bar{1}0)$, and $(\bar{3}31)$ points using your Wulff net: they all lie on one great circle because they are in the same zone. Now identify the zone axis directly by measuring 90° from all the poles. The result is of course the same.

- Notice that if you used the stereographic technique with a noncubic material, you would locate a direction not a plane normal.
- You can make the determination of **B** more accurate by making **s** = 0 for each reflection you use and then estimating your deviation from this idealized orientation. If the specimen is thicker, use Kikuchi lines (Chapter 19).

18.9. ORIENTATION RELATIONSHIPS

Once you've learned how to index a DP and determine **B**, you can determine *orientation relationships*, which are one of the most useful aspects of diffraction in the TEM for the metallurgist. The orientation relationship (OR) between

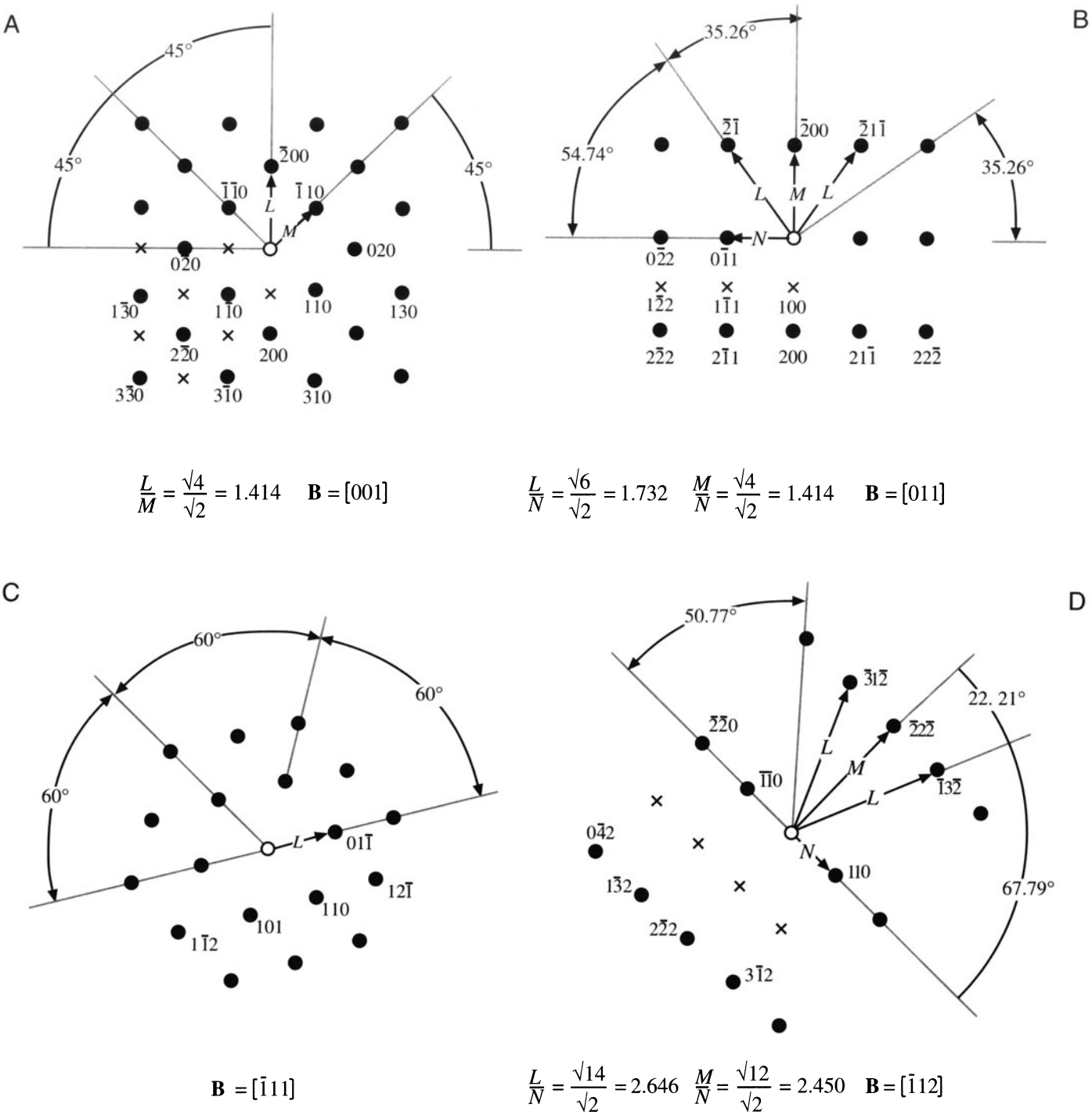

$\frac{L}{M} = \frac{\sqrt{4}}{\sqrt{2}} = 1.414 \quad \mathbf{B} = [001]$

$\frac{L}{N} = \frac{\sqrt{6}}{\sqrt{2}} = 1.732 \quad \frac{M}{N} = \frac{\sqrt{4}}{\sqrt{2}} = 1.414 \quad \mathbf{B} = [011]$

$\mathbf{B} = [\bar{1}11]$

$\frac{L}{N} = \frac{\sqrt{14}}{\sqrt{2}} = 2.646 \quad \frac{M}{N} = \frac{\sqrt{12}}{\sqrt{2}} = 2.450 \quad \mathbf{B} = [\bar{1}12]$

Figure 18.17. Four standard indexed diffraction patterns for bcc crystals in the [001], [011], [$\bar{1}$11], and [$\bar{1}$12] beam directions. Ratios of the principal spot spacings are shown as well as the angles between the principal plane normals. Forbidden reflections are indicated by x.

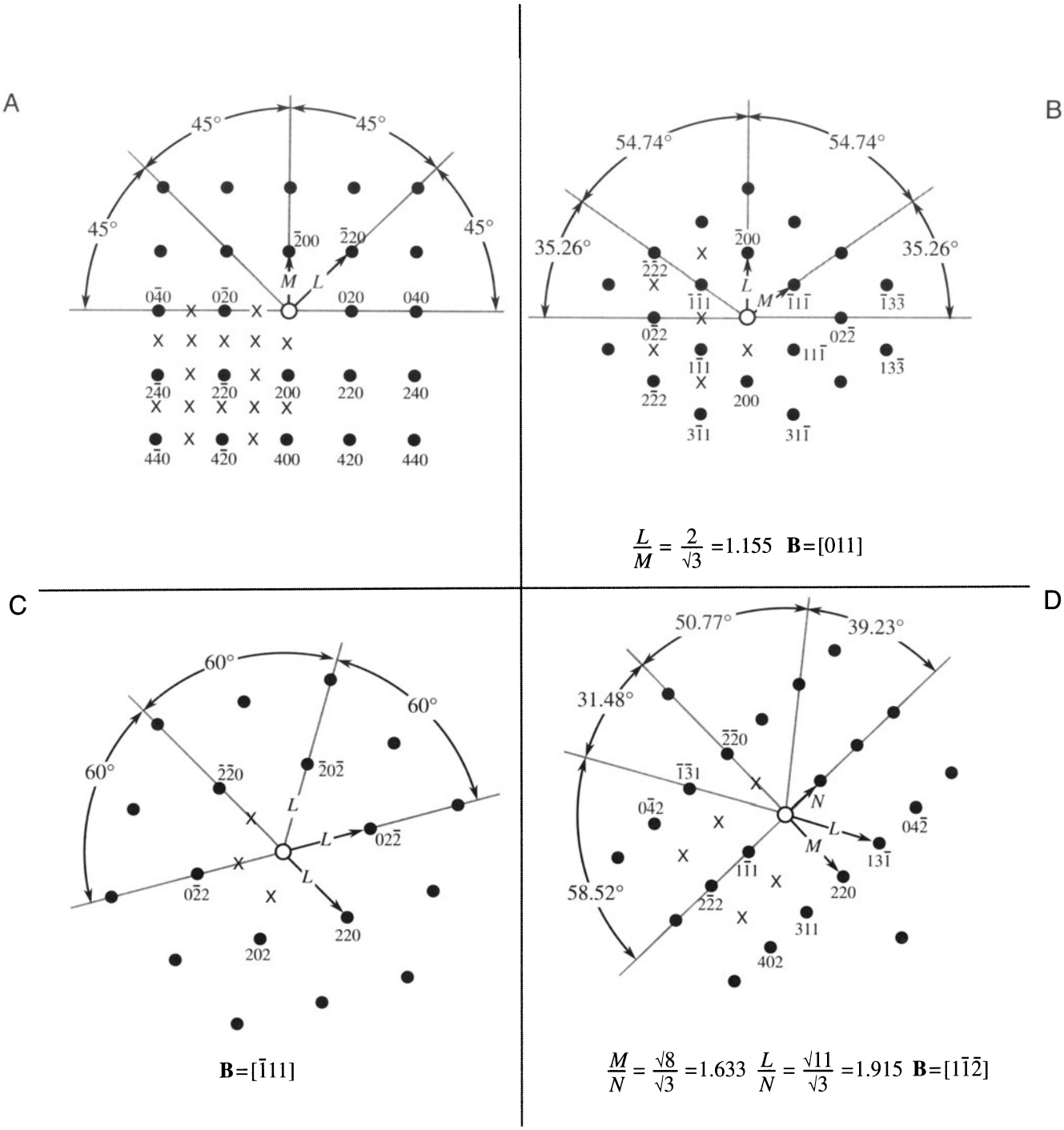

Figure 18.18. Four standard indexed diffraction patterns for fcc crystals in the [001], [011], [$\bar{1}$11], and [$\bar{1}$12] beam directions. Ratios of the principal spot spacings are shown as well as the angles between the principal plane normals. Forbidden reflections are indicated by x.

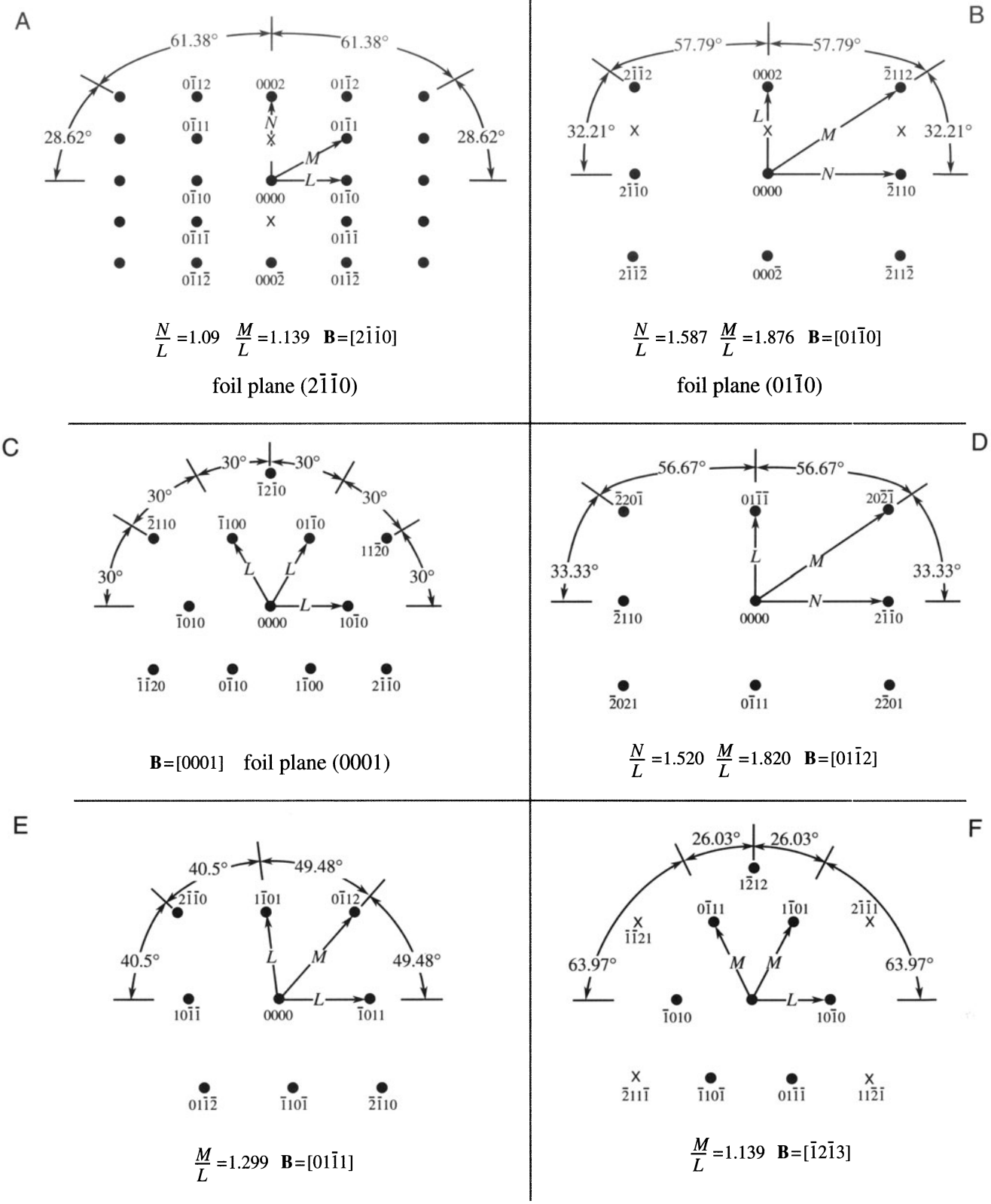

Figure 18.19. Six standard indexed diffraction patterns for hcp crystals in the [2$\bar{1}\bar{1}$0], [01$\bar{1}$0], [0001], [01$\bar{1}$2], [01$\bar{1}$1], and [1$\bar{2}\bar{1}\bar{3}$] beam directions. Ratios of the principal spot spacings are shown as well as the angles between the principal plane normals. Forbidden reflections are indicated by x.

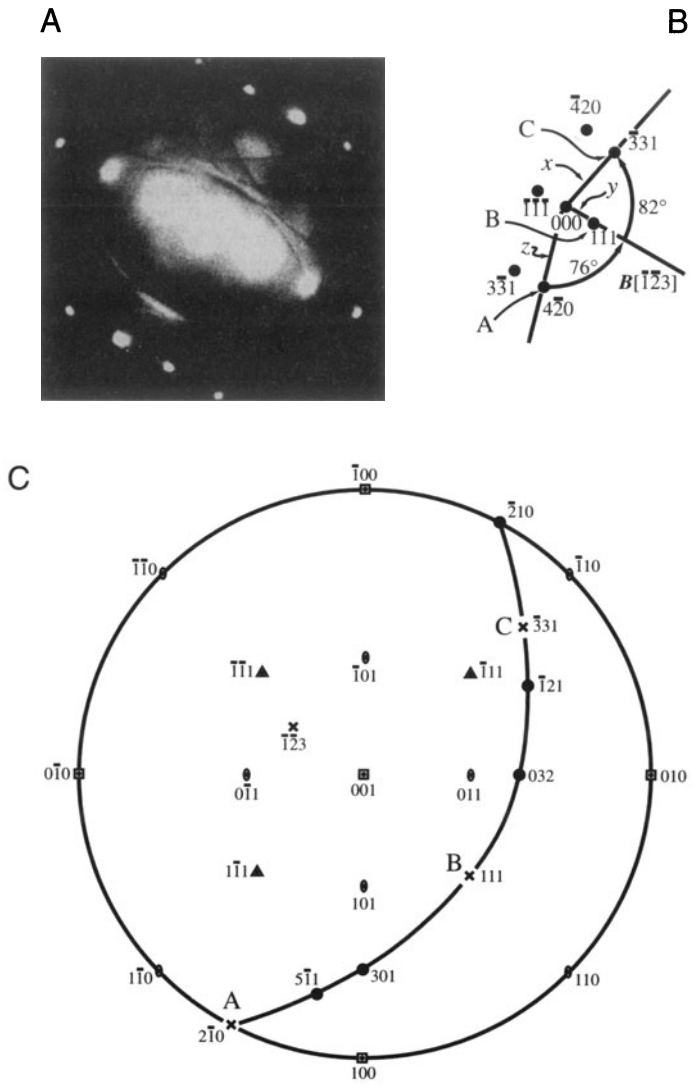

Figure 18.20. (A) An fcc pattern, indexed in (B) with the major indexed poles plotted on a stereographic projection in (C), identifying the pole of the great circle as $\bar{1}\bar{2}3$, which is therefore the beam direction for the pattern in (A).

two different crystals is important in many materials. We often want to know how a precipitate is oriented relative to its surrounding matrix, a fiber to the adjacent matrix, a thin film to the substrate, or two grains are oriented either side of a GB. The OR can be described in one of two ways:

- Two directions or plane normals (or two sets of parallel planes) can be parallel in the two crystals (the parallel-plane/direction relationship). We use this description for precipitate-matrix (β-α) orientation relationships where the crystal systems may be different.
- The two crystals have a common direction (axis) so that one crystal can be rotated through some angle into exact alignment with the other (an axis-angle pair). We use this for GBs where the same material is present either side of the boundary.

Record a set of three DPs, one from each crystal and one including the interface. If you're lucky you'll be able to index both single-crystal patterns directly. If one of them shows too few spots, you should try to record a complementary Kikuchi pattern or CBED pattern to provide more information. With CBED patterns from very small regions, you'll have to take a pattern in one crystal, translate the specimen, and take another pattern from the other grain.

We'll go through the experimental steps for analyzing the parallel-plane/direction relationship for two phases α and β:

- Tilt to zone-axis pattern (ZAP) 1 in phase α, the matrix phase. Record and index it to determine $\mathbf{B}_1(\alpha)$.
- Translate the precipitate, β, onto the axis without touching the beam-tilt controls and record another DP. This pattern may not be exactly on a zone axis, so it may be more difficult to index; then Kikuchi lines may help considerably. Nevertheless, you need to determine a parallel beam direction, $\mathbf{B}_1(\beta)$, for the precipitate.
- Translate back to the matrix. Tilt the specimen in a known direction until you find a different ZAP (again Kikuchi maps from the next chapter will help you do this). Record and index ZAP 2 to give $\mathbf{B}_2(\alpha)$.
- Translate back to the precipitate, record the DP and index it, giving you $\mathbf{B}_2(\beta)$.
- Plot the position of $\mathbf{B}_1$ and $\mathbf{B}_2$ for both α and β on a stereogram and construct the poles of the important planes that are normal to each **B**. These will be the low-index planes that you indexed in each pattern.

So now you know that $\mathbf{B}_1(\alpha)$ is parallel to $\mathbf{B}_1(\beta)$ and $\mathbf{B}_2(\alpha)$ is parallel to $\mathbf{B}_2(\beta)$. You can also see which plane normals are parallel (if any) from the stereogram. So you can quote the OR in terms of these two pairs of parallel directions, or a pair of directions and a pair of plane normals in the zone of each **B**. It may well be the case that you can't find two low-index planes or directions that are parallel, in which case the orientation relationship is not a strong one. However, there are some well-known ORs between phases that you should know:

- Best known is the *cube/cube* OR. If an fcc precipitate forms inside an fcc matrix (e.g., Al_3Li

(δ') in an Al-Li (α) solid solution), then we find:

$[100]_{\delta'}$ is parallel to $[100]_{\alpha}$,
$(010)_{\delta'}$ is parallel to $(010)_{\alpha}$.

Obviously, in these circumstances, any two <*UVW*> directions or $\{hk\ell\}$ planes in the cubic system would be parallel. It's just convention to choose the lowest-index planes or directions to define the OR. When the lowest-index planes and directions align, the surface energy between the phases tends to be lowest, so this configuration is thermodynamically favored.

- The Kurdjumov–Sachs OR is often found relating fcc and bcc crystalline grains. The close-packed planes (or closest packed in bcc) and close-packed directions are parallel, but these are not now identical.

  $(111)_{fcc}$ is parallel to $(011)_{bcc}$ (the closest-packed planes),
  $[10\bar{1}]_{fcc}$ is parallel to $[11\bar{1}]_{bcc}$ (the close-packed directions),
  $(\bar{1}2\bar{1})_{fcc}$ is parallel to $(\bar{2}1\bar{1})_{bcc}$.

- The Nishiyama–Wassermann OR is related to the Kurdjumov–Sachs OR:

  $[0\bar{1}1]_{fcc}$ is parallel to $[001]_{bcc}$,
  $(\bar{1}11)_{fcc}$ is parallel to $(\bar{1}10)_{bcc}$ (the closest-packed planes),
  $(211)_{fcc}$ is parallel to $(110)_{bcc}$.

  If you plot this out on a stereogram, you'll see it's only a few degrees away from the Kurdjumov–Sachs relationship.

- The fcc and hcp systems also share an OR in which the close-packed planes and directions are parallel:

  $(111)_{fcc}$ is parallel to $(0001)_{hcp}$ (the close-packed planes),
  $[1\bar{1}0]_{fcc}$ is parallel to $[1\bar{2}10]_{hcp}$ (the close-packed directions).

If you want to determine an axis-angle pair, you proceed in a similar way. Obtain two indexed beam directions, $\mathbf{B}_1$ and $\mathbf{B}_2$, in each crystal, and plot them on a stereogram. Then you need to determine from the stereogram which angle brings the directions and planes from one crystal into coincidence with the other crystal.

There's a full discussion of this method and some more examples of ORs in Edington (1976).

18.10. COMPUTER ANALYSIS

Although you must be able to analyze and index DPs "by hand," it's likely that you'll use one of the many software packages to help you with any material, especially if it is not cubic. The main challenge comes when you have to index the DP of a new material. Your laboratory should have the standard reference sources listed at the end of the chapter. The approach simply requires that you collect all the data you can and then search through the PDF files, or better still the NIST/Sandia/ICDD electron-diffraction database, until you find a match. Yes, it is a lot of work and you have to remember some rules:

- Measurements made on calibrated SAD patterns will be accurate to 1–2%. If you think you're more accurate, you may eliminate the material you're seeking from your database search!
- Check for multiple domains and double diffraction first. An example of such a DP is shown in Figure 18.21. As you can appreciate from the schematic, you must be careful not to confuse such patterns with those showing systematic absences.

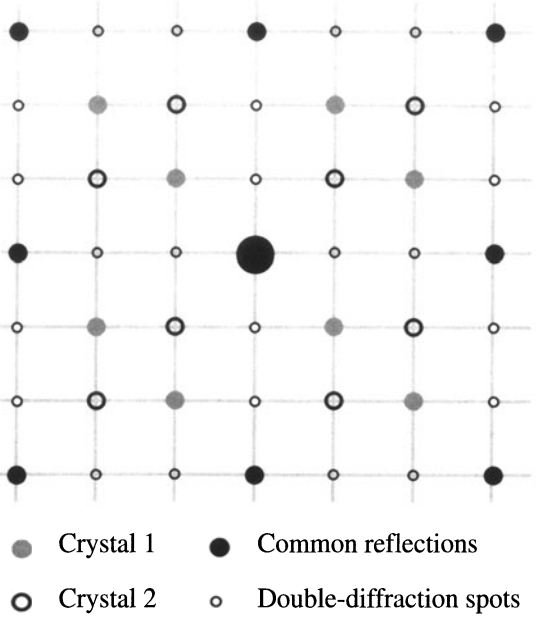

Figure 18.21. Care is needed to recognize diffraction from two similar domains, which appears identical to diffraction from a real structure with a different symmetry. All the spots lie on a square array which may lead to erroneous indexing as a 100 pattern. The DP actually consists of separate patterns from two overlapping crystals, plus double-diffraction spots as indicated.

A strategy for search-and-match procedures has been given by Lyman and Carr (1992). The goal of the exercise is to identify all the possible compounds that could produce your DP. Then you can use other data (e.g., the

chemistry deduced by XEDS or EELS) to make the final identification. Computers not only give us the speed to make such searches possible, but are also more objective. The procedure has four simple steps:

- Obtain reliable data (and do not be too optimistic or overconfident in your accuracy).
- Search the database for possible matches. With the right database, chemical information will help.
- Test the matches you find. Are any of them possible?
- Confirm the identification. Now you can go back to the microscope and use CBED to explore symmetry elements, improve your lattice-parameter measurements, etc. (Chapters 20 and 21). You can also simulate the DPs to confirm that the popular software packages do reproduce what you see.

CHAPTER SUMMARY

This chapter has been concerned almost entirely with experimental technique.

- The stereographic projection is a very helpful aid. It's similar to projections we use to map the earth. Diffraction space (like global space) is three-dimensional. The stereographic projection gives us a two-dimensional map to guide us from pole to pole!
- How do you obtain the best DP from your specimen? Use the right exposure, always focus the DP, and use the best technique (CBED or SAD) for the size of the area of interest.
- Take the trouble and time always to get good DPs. You never know when you'll really need that information and an extra 9 or 29 seconds exposure time is not long, considering how long you'll spend analyzing the results!
- Which type of DP should you use? This depends on the characteristics of your specimen and what you want to know.
- Remember that reflections with moderately large values of **g** should give you the best value for both d and ϕ, but be absolutely sure that $\mathbf{s} = 0$ for your chosen **g**.
- DPs from polycrystalline and amorphous materials contain a wealth of information. The added value that TEM brings over X-ray diffraction is the spatial resolution and the accompanying images.
- Computer indexing of DPs will be the norm and will be automatic if you know your material. If you understand the principles discussed here you will avoid a few pitfalls. Finally, we'll repeat our word of caution: there is a very famous paper on interstitial defects in a ceramic and a follow-up paper on vacancy defects. The first paper missed the 180° ambiguity in the DP!

REFERENCES

General References

Andrews, K.W., Dyson, D.J., and Keown, S.R. (1971) *Interpretation of Electron Diffraction Patterns,* 2nd edition, Plenum Press, New York. An essential resource for anyone using electron diffraction.

Burger, M.J. (1978) *Elementary Crystallography,* MIT Press, Cambridge, Massachusetts. One of the classics.

Cullity, B.D. (1978) *Elements of X-ray Diffraction,* 2nd edition, Addison-Wesley, Reading, Massachusetts. The standard text on X-ray analysis.

Edington, J.W. (1976) *Practical Electron Microscopy in Materials Science,* Van Nostrand Reinhold, New York. Part 2 of the book is full of useful hints and examples.

Giacovazzo, C., Monaco, H.L., Viterbo, D., Scordari, F., Gilli, G., Zanotti, G., and Catti, M. (1992) *Fundamentals of Crystallography,* Oxford University Press and IUCr. Oxford. A comprehensive reference book.

Glazer, A.M. (1987) *The Structure of Crystals,* Adam Hilger, Bristol, United Kingdom. The essentials condensed into a 50-page monograph.

Hammond, C. (1992) *Introduction to Crystallography,* 2nd edition, Royal Microscopical Society, Oxford, United Kingdom. An excellent compact introduction to the subject with a nice section on the biographies of crystallographers.

Johari, O. and Thomas, G. (1969) *The Stereographic Projection and its Applications in Techniques of Metals Research,* (Ed. R.F. Bunshah), Interscience, New York. A very helpful book if you can find a copy.

Kelly, A. and Groves, G.W. (1970) *Crystallography and Crystal Defects,* Addison-Wesley, Reading, MA. The original out-of-print 1970 edition has been reprinted by TechBooks, 4012 Williamsburg Court, Fairfax, Virginia 22032. A classic which all materials scientists should already have on their shelves. This is not only the standard introductory text on this subject but also gives a good review of the stereographic projection.

Klein, C. and Hurlbut, C.S. (1985) *Manual of Mineralogy,* Wiley, New York. This is the modern version of the original classic by James D. Dana. It gives an excellent readable review of the stereographic projection and its relation to the globe plus basic crystallography.

Smaill, J.S. (1972) *Metallurgical Stereographic Projections,* Adam Hilger Ltd., London. Chapter 20 is another source for stereographic projections and the Wulff net.

Vainshtein, B.K. (1981) *Modern Crystallography,* **I–IV**, Springer-Verlag, New York.

Specific References

Cockayne, D.J.H., McKenzie, D., and Mueller, D. (1991) *Microscopy, Microanalysis, Microstructure* **2,** 359.

Graczyk, J.F. and Chaudhari, P. (1973) *Phys. Stat. Sol.* **b58,** 163.

Howie, A. (1988) in *High-Resolution Transmission Microscopy and Associated Techniques* (Eds. P. Buseck, J. Cowley, and L. Eyring), p. 607, Oxford University Press, New York.

Lyman, C.E. and Carr, M.J. (1992) in *Electron Diffraction Techniques,* **2** (Ed. J.M. Cowley), p. 373, Oxford University Press, New York.

Randle, V. (1993) *The Measurement of Grain Boundary Geometry,* Institute of Physics, Bristol, United Kingdom.

Rudee, M.L. and Howie, A. (1972) *Phil. Mag.* **25,** 1001.

Tietz, L.A., Carter, C.B., and McKernan, S. (1995) *Ultramicroscopy* **60,** 241.

Vainshtein, B.K., Zuyagin, B.B., and Avilov, A.V. (1992) in *Electron Diffraction Techniques,* **1** (Ed. J.M. Cowley), p. 216, Oxford University Press, New York.

References for Crystallographic Data

Stereographic projections and the Wulff net can be obtained from SPI Supplies, P.O. Box 656, Westchester, Pennsylvania 19831-0656 (1-800 242 4774).

Donnay, J.D.H. and Ondik, H.M. (1972) *Crystal Data: Determinative Tables,* 3rd edition, National Bureau of Standards, US Dept. of Commerce, Washington, DC. This source lists the ratios of lattice parameters for different materials.

Wells, A.F. (1984) *Structural Inorganic Chemistry,* 6th edition, Oxford University Press, New York. The source for crystal-structure data in inorganic materials.

Villars, P. and Calvert, L.D. (1985) *Pearson's Handbook of Crystallographic Data for Intermetallic Phases*, ASM, Metals Park, Ohio is now in many volumes covering an ever-growing number of materials.

ICDD Powder Diffraction File is produced by the International Center for Diffraction Data (Swarthmore, Pennsylvania, 1990). It is available in various formats. Most researchers favor the CD-ROM version.

ICDD Elemental and Lattice Spacing Index is produced by the same Center but is only presently available in printed form. This index used to be known as the ASTM cards (3" by 5" index cards!). Each file gives the *d*-spacings and X-ray diffraction peak intensities. These files should be in a more useful computer-accessible form.

NIST Crystal Data can be purchased as a CD-ROM or on tape. Parts are from the Donnay-Ondik books (see above). A program called NBS*SEARCH will allow you to search this database. These files give not only crystallographic data but also physical data on more than 100,000 organic and inorganic materials. Obtainable from NIST Crystal Data Center, NIST, Gaithersburg, MD 20899.

NIST/Sandia/ICDD Electron Diffraction Database has become available thanks to the tireless efforts of M. Carr, who has also provided methods for searching this database on a PC.

Desktop Microscopist (see Section 1.5). This program can look up crystal data and plot out the diffraction pattern.